Hindawi Publishing Corporation Advances in Nonlinear Optics Volume 2008, Article ID 480362, 10 pages doi:10.1155/2008/480362

Research Article

Parabolic Pulse Generation Using Tapered Microstructured Optical Fibres

Natasha Vukovic, Neil G. R. Broderick, and Francesco Poletti

Optoelectronics Research Centre, University of Southampton, Southampton SO17 1BJ, UK

Correspondence should be addressed to Natasha Vukovic, ntv@orc.soton.ac.uk

Received 21 September 2007; Accepted 20 December 2007

Recommended by Stephane Coen

This paper presents a numerical study of parabolic pulse generation in tapered microstructured optical fibres (MOFs). Based on our results and the algorithms presented, one can determine the linear taper profile (starting and finishing pitch values and taper length) needed to achieve parabolic pulse shaping of an initial Gaussian pulse shape with different widths and powers. We quantify the evolution of the parabolic pulse using the misfit parameter and show that it is possible to reach values significantly better than those obtained by a step index fibre.

Copyright © 2008 Natasha Vukovic et al. This is an open access article distributed under the Creative Commons Attribution License, which permits unrestricted use, distribution, and reproduction in any medium, provided the original work is properly cited

1. INTRODUCTION

The generation of parabolic pulse has been widely investigated and is still an active area of research due to its unique properties and numerous applications. In the normal dispersion regime, due to the interaction between dispersive and nonlinear effects, a high intensity pulse suffers wave breaking, manifesting itself as oscillations on the pulse's tail [1]. However, for a linearly chirped parabolic pulse, this effect can be avoided if the pulse's chirp is such that the rate of change of the time separation is the same for all parts of the pulse, resulting in the pulse evolving in a self-similar fashion [1]. Importantly, linearly chirped parabolic pulses can be efficiently compressed and are used in many telecommunications applications such as optical regeneration [2] or temporal Fourier transforms [3]. Such pulses are useful for applications such as pulse compression, and indeed compression of picosecond pulses down to femtosecond range has been experimentally demonstrated in [4, 5].

Different approaches to the generation of parabolic pulses have been studied and include a fibre Bragg grating [4], dispersion decreasing fibre in the normal dispersion regime [6], normally dispersive two-segment fibre device [7–9], optical amplifiers [10], or similariton lasers [11]. Applications requiring high-power parabolic pulses often rely on an

optical amplifier as parabolic pulses are automatically generated in these amplifiers. On the other hand, there is a range of applications, particularly related to optical signal processing, where a high signal power is undesirable, since it requires a high-power pump source and adds costs and complexity to the system [7]. Another drawback of using an active system is that it introduces amplified spontaneous emission noise. Hence, the need for other ways to generate parabolic pulses using passive fibres is required.

The passive means to generate parabolic pulses described above all require relative long lengths of fibre (>1 km) and are suitable for picosecond pulse widths (>1picosecond). In [12], however, it was shown that by using a comb-like dispersion a decreasing profile also leads to parabolic pulse generation, in a few metres of fibre. Such comb-like profiles are complicated to produce (relying on multiple splices), and hence there is a need for a different approach for efficient generation of parabolic pulses in relative short lengths and with the flexibility of coping with different input pulse widths and energies. Due to the exceptional properties of microstructured optical fibres such as control of optical properties (dispersion, nonlinearity, and birefringence), "endlessly" single-mode guidance, extreme mode sizes, low bend loss [13], we chose to examine microstructured optical fibrebased tapers for parabolic pulse generation. Tapered MOFs have found many other applications, such as pulse compression [14, 15], supercontinuum generation [16], generating soliton frequency shift [17], and SBS threshold enhancement [18].

Our aim here is to investigate whether tapered microstructured fibres can be used to efficiently generate parabolic pulses in short lengths (<10 m). We choose to taper the fibres, since, as it was pointed out in [6, 19-21], that in a system described by the ideal lossless nonlinear Schrodinger equation (NLSE) with decreasing dispersion, optical pulse evolution is formally similar to that of a medium with a constant gain. As a consequence, an asymptotic self-similar parabolic pulse solution is found to exist in a dispersion decreasing fibre with normal group velocity dispersion, that is, a taper [6]. Using linear dispersion profiles, we achieved parabolic pulses after a finite propagation length, with the parabolic pulse remaining stable for some length before being distorted. Formally, this approach does not correspond to an asymptotic self-similar parabolic pulse, since we used a linear taper profile and not a hyperbolic dispersion profile. However, our approach is still based on the observation that the longitudinal decrease of the normal dispersion is formally equivalent to optical gain.

Section 2 presents results of modelling and simulation of normally dispersive microstructured optical fibres. We have identified two normal dispersion regions, and outlined a procedure for choosing the parameters of the taper profile (starting and finishing values of the pitch) and the air-filling factor, for efficient pulse generation. Then in Section 3, using the NLSE, we show how initial Gaussian pulses of different input powers and widths evolve into parabolic pulses with a linear chirp for two different tapers. Results are quantified using the misfit parameter, which measures the root mean square error between the propagated pulse and its parabolic fit in the time domain, and presented so that the optimum taper length that corresponds to the best parabolic pulse can be determined. The best misfit distances for both regions and a range of pulse power and initial pulse widths are given, allowing one to choose the best taper profiles for a wide range of initial pulse parameters.

2. MOF AND TAPER MODELLING

A microstructured fibre consists of a periodic array of airholes with a central defect acting as the core with the optical parameters of the fibre being completely determined by the period Λ and the relative air-hole size d/Λ . We used the finite element method (FEM), implemented in the commercial software package Comsol Multiphysics, to solve for dispersion, effective area, and confinement loss of the lowestorder mode. The FEM elements are flexible from a geometric point of view (easy treatments of any shape of structure) and from the material point of view (it allows inhomogeneous, anisotropic, or nonlinear characteristics to be incorporated) [22]. The refractive index of silica $n(\omega)$ is approximated by the standard Sellmeier equation [23]. The geometry of the MOF used was a hexagonal pattern with 11 layers of holes, (see Figure 1). Group theory analysis allows only a quarter of the structure to be simulated with no loss of information

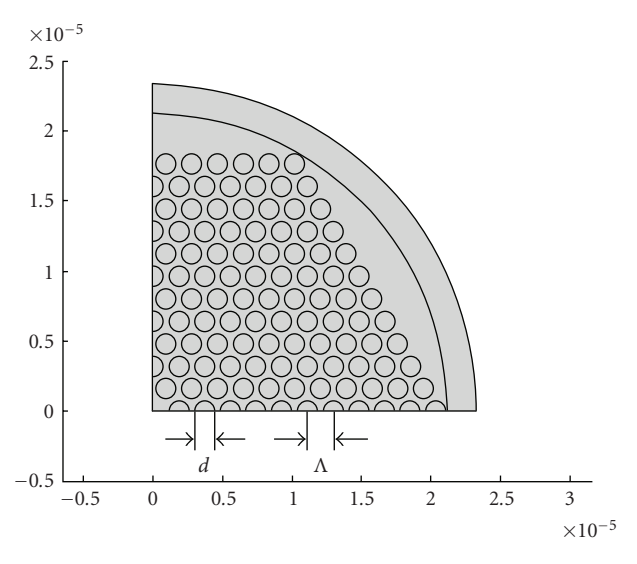


FIGURE 1: Cross-section of the MOF with 11 rings of holes (d-hole diameter, Λ -pitch).

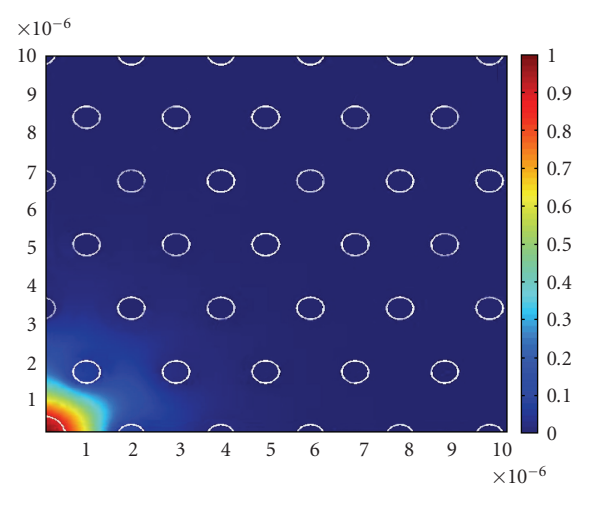


FIGURE 2: The magnitude of the Poynting vector.

about the modes saving considerable amount of the computational time [24]. A typical fundamental mode of a MOF, for illustrative purposes, is shown in Figure 2. Note that the light is well confined to the core region and penetrates only slightly into the cladding region.

For this study, the crucial result of the fibre simulations is the propagation constant β and associated effective index $n_{\rm eff}$ which are related by

$$\beta = \frac{2\pi n_{\text{eff}}}{\lambda}.\tag{1}$$

Note that for a finite structure, $n_{\rm eff}$ is a complex number with the imaginary part giving the confinement loss of the mode. In our FEM analysis, we used a perfectly matched layer (PML) to treat the open boundaries. Using the complex effective index, the confinement loss is calculated as

$$CL [dB/m] = \frac{20 \times 10^6}{\ln 10} \frac{2\pi}{\lambda [\mu m]} Im(n_{\text{eff}}). \tag{2}$$

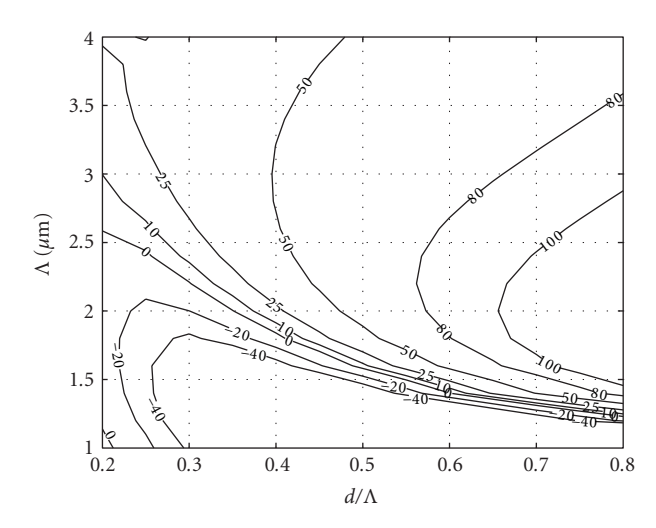


Figure 3: Dispersion (D) contour plot at $\lambda = 1.55 \,\mu\text{m}$.

For useful fibres, a loss of less than 1 dB/m is needed and this forces us to reduce the parameter space of possible fibres in our study.

The chromatic dispersion, d, of the fibre is given by

$$D = -\frac{2\pi c}{\lambda^2} \beta_2, \tag{3}$$

where β_n is a group velocity dispersion defined as follows:

$$\beta_2 = \frac{d^2 \beta}{d\omega^2}.\tag{4}$$

Note that as pure silica at 1.55 microns has positive dispersion, and so fibres with large negative waveguide dispersion are needed in this study.

Since ideal MOFs depend on only two parameters, their optical properties can be best displayed using an optical map such as that shown in Figure 3 which shows the dispersion of various MOFs at 1.55 µm (wavelength mostly used in telecommunications applications). This plot enables us to find the range of values for Λ and d/Λ that would provide normal dispersion regime (D < 0) of the fibre. It can be seen that almost any value of d/Λ can be used assuming that the correct value of Λ is chosen and so we need to choose a range that can be easily fabricated. Importantly, the dispersion characteristics of any fibre taper can be immediately read off the contour graph as each fibre taper corresponds to a path in $(\Lambda, d/\Lambda)$ space. However, for ease of taper fabrication, only vertical paths are considered here as they correspond to fibre tapers with a constant d/Λ which can be made by simply heating and stretching the fibre. More complicated profiles which can be made by pressuring the taper during fabrication are not considered here.

Since our fibre tapers have a fixed d/Λ , we can compress the 2D map in Figure 3 into a series of overlapping curves as shown in Figure 4.

In Figure 4, the dispersion is calculated versus air-filling factor d/Λ , for different values of parameter Λ . From Figure 4, it can be seen that there are several regions of d/Λ

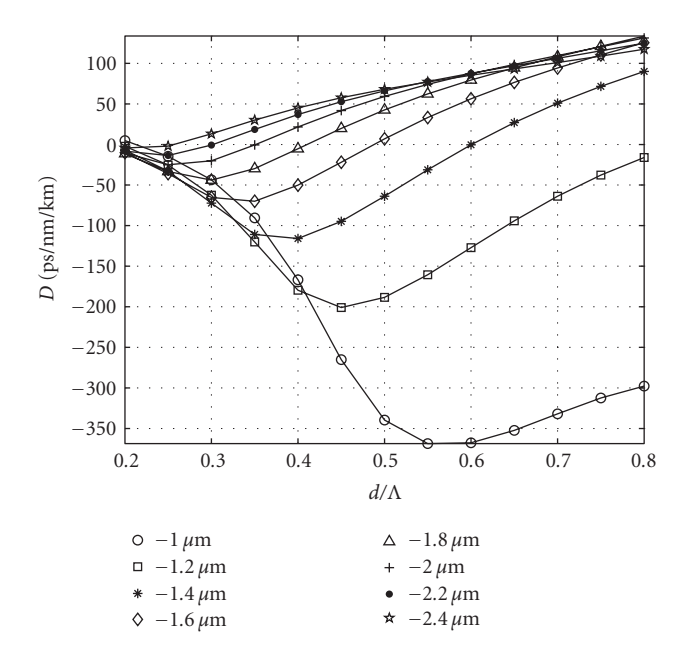


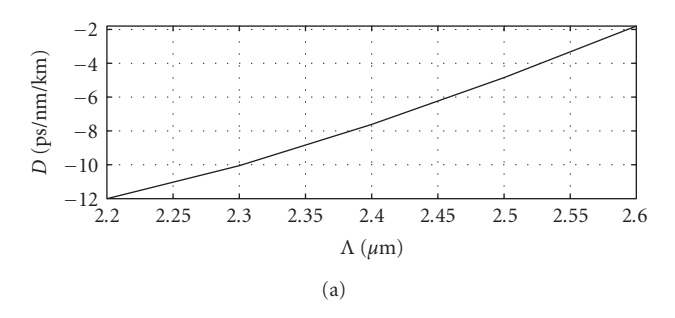
Figure 4: Dispersion versus d/Λ for different values of Λ .

that can be chosen so that a fibre operates in the normal dispersion regime. We chose to examine three regions with $d/\Lambda = 0.2$, 0.3, and 0.8, respectively, as these regions have a low absolute value of dispersion. Both the nonlinearity and the third-order dispersion differ by an order of magnitude in the different regions. Thus, these regions allow us to observe the effects of different fibre parameters on the pulse shaping.

For these regions, we determined the maximum and minimum values of Λ , in accordance with the limits that absolute value of the dispersion is lower than $-40\,\mathrm{ps/nm/km}$ (as this level of dispersion can be acceptable in communications applications), according to Figure 3. We next examined the effect of the confinement loss for each region. Figure 5 shows plots of the dispersion and confinement loss versus pitch (Λ) for a fixed $d/\Lambda=0.2$. Similarly, Figures 6 and 7 show the results for $d/\Lambda=0.3$ and $d/\Lambda=0.8$, respectively.

From Figures 5–7, we can see that although the dispersion is limited to the absolute value of 40 ps/nm/km, the confinement loss changes by several orders of magnitude for different d/Λ values, being the lowest for $d/\Lambda=0.8$ and the highest for $d/\Lambda=0.2$ (as expected). The results obtained for $d/\Lambda=0.2$ show that although the dispersion is low, the confinement loss of up to 100 dB/m is the crucial factor making this region useless for practical experiments. Therefore, we will concentrate on the regions of $d/\Lambda=0.3$ and $d/\Lambda=0.8$, as both the dispersion and the confinement loss lie within acceptable limits.

From Figure 6, we choose the parameters of the first taper, with starting pitch $(1.85\,\mu\text{m})$ and finishing pitch $(2.2\,\mu\text{m})$ In the same manner, from Figure 7, we chose parameters of the second taper, the starting pitch $(1.18\,\mu\text{m})$ and finishing pitch $(1.22\,\mu\text{m})$. Even knowing the starting and finishing values of the dispersion, there is still an infinite range of possible tapers to consider. For the sake of simplicity, we



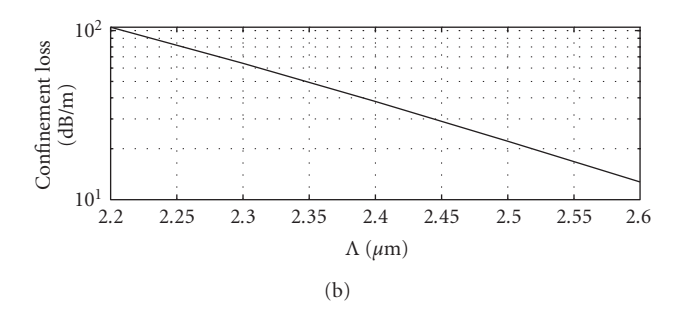
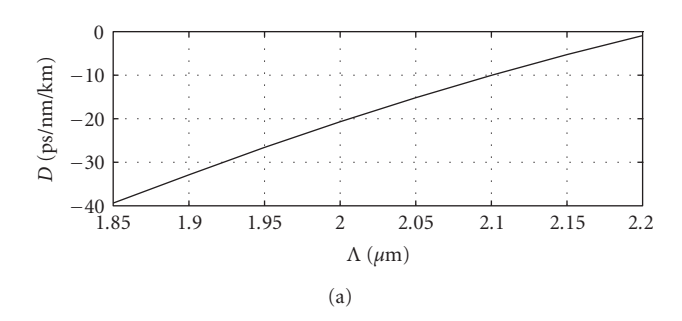


Figure 5: Dispersion and confinement loss versus pitch, when $d/\Lambda = 0.2$.



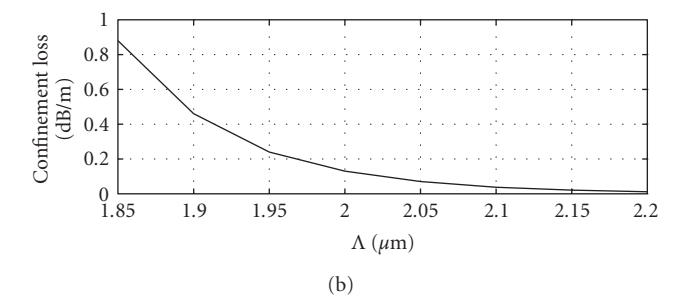


Figure 6: Dispersion and confinement loss versus pitch, when $d/\Lambda = 0.3$.

choose a linear profile for the taper, determined by fibre pitch at the beginning and the end, from the equation

$$\Lambda(z) = \frac{(z_{\text{max}} - z)\Lambda(0) + z\Lambda(z_{\text{max}})}{z_{\text{max}}},$$
 (5)

where z_{max} is the taper length, $\Lambda(0) = 1.85 \, \mu\text{m}$, and $\Lambda(z_{\text{max}}) = 2.2 \, \mu\text{m}$. In the normal dispersion regime, smaller absolute values of dispersion correspond to larger core diameters, and therefore taper should be used from the narrow end. Other taper profiles are possible (such as exponentially decreasing profiles that will be studied in a later paper).

The parameters of the MOF that change with tapering are the chromatic dispersion β_2 , third-order dispersion β_3 , and nonlinear coefficient γ . The nonlinear coefficient γ is given by [20]

$$\gamma = \frac{2\pi n_2}{\lambda A_{\text{eff}}},\tag{6}$$

where $n_2 = 2.2 \times 10^{-20} \, \mathrm{m^2/W}$ is the nonlinear refractive index of the silica fibre, A_{eff} is the effective mode area, and λ is the optical wavelength. Note that it is the effective area that changes along the taper and hence γ does as well. Tables 1 and 2 summarize taper parameters for regions $d/\Lambda = 0.3$ and $d/\Lambda = 0.8$, respectively.

The final linear taper profile and change of parameters β_2 , β_3 , and γ with the distance are shown in Figures 8 and 9 for $d/\Lambda = 0.3$ and $d/\Lambda = 0.8$, respectively.

3. SIMULATIONS AND DISCUSSION

Having chosen the fibre tapers, the next step is to examine optical propagation through them. The propagation of

pulses in an optical fibre with variable dispersion and nonlinearity is described by nonlinear Schrödinger equation (NLSE) [23]:

$$\frac{\partial u}{\partial z} + \frac{\alpha}{2}u + i\frac{\beta_2(z)}{2!}\frac{\partial^2 u}{\partial t^2} - \frac{\beta_3(z)}{3!}\frac{\partial^3 u}{\partial t^3} - i\gamma(z)|u|^2u = 0, \quad (7)$$

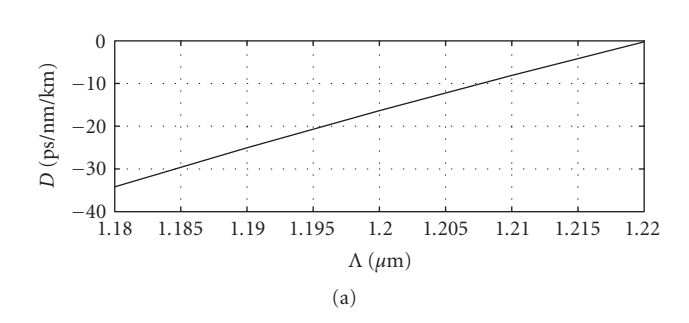
where u is the complex electric field envelope, z is the distance along the fibre, t is retarded time and is defined such that for any distance z along the fibre, the centre of the pulse is at t=0, α is fibre loss, β_2 is group velocity dispersion, β_3 is third-order dispersion, and y is the nonlinear coefficient. We solved the NLSE (7) numerically, using the symmetrized split-step Fourier method [23, 25], for our two tapers. In order to quantify the evolution towards parabolic pulse, we computed the evolution of the misfit parameter M^2 between the pulse intensity profile $|u|^2$ and the parabolic fit $|p|^2$, using [7]

$$M^{2} = \frac{\int [|u|^{2} - |p|^{2}]^{2} d\tau}{\int |u|^{4} d\tau},$$
 (8)

where p(t) is the generalized expression for the parabolic pulse

$$p(t) = \begin{cases} \sqrt{P_p} \sqrt{1 - 2\frac{t^2}{T_p^2}} \exp\left(-i\frac{C}{2}t^2\right), & \text{if } |t| \le \frac{T_p}{\sqrt{2}}, \\ 0, & \text{elsewhere,} \end{cases}$$
(9)

where P_p is the peak power of the pulse, T_p is the temporal full-width at half maximum (FWHM), and C is the linear chirp coefficient. We also use a local misfit parameter which looks at the difference between the pulse and an ideal parabolic pulse at a particular instant in time.



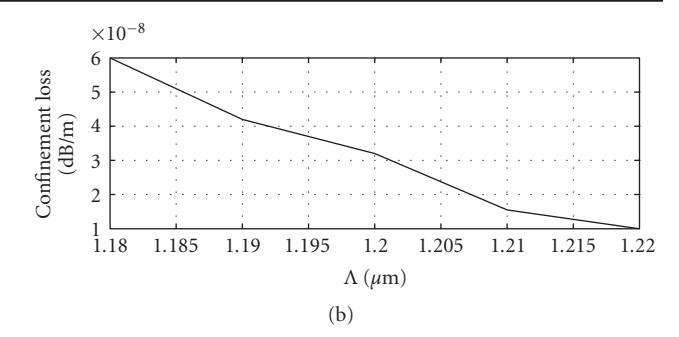
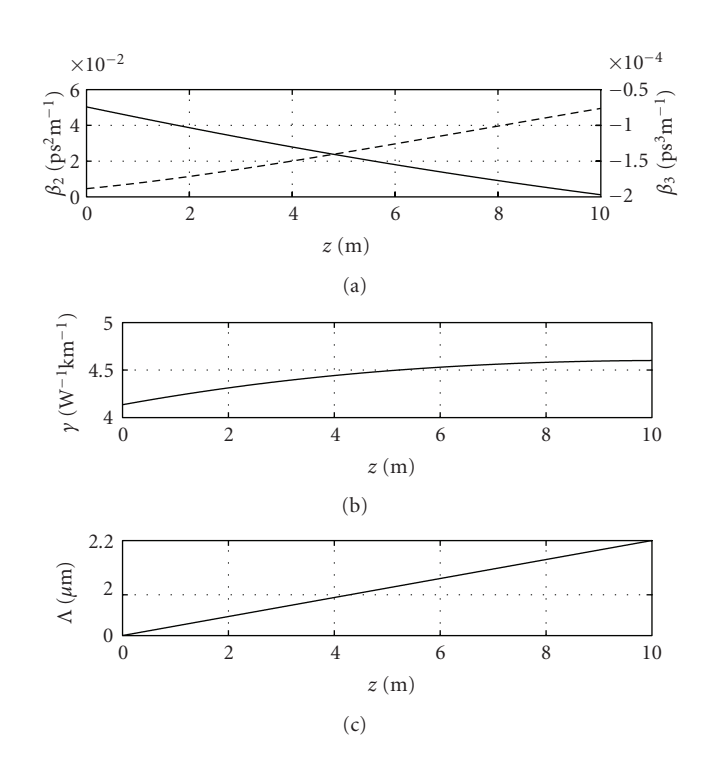


Figure 7: Dispersion and confinement loss versus pitch, when $d/\Lambda = 0.8$.

Table 1: Parameters of the tapered fibre $(d/\Lambda = 0.3)$.

	Λ [μm]	$\beta_2 [ps^2/m]$	$\beta_3 [ps^3/m]$	$\gamma[\mathrm{W}^{-1}\mathrm{km}^{-1}]$
Start	1.85	0.050367	-0.0001886	4.135
End	2.2	0.001167	-0.0000761	4.6



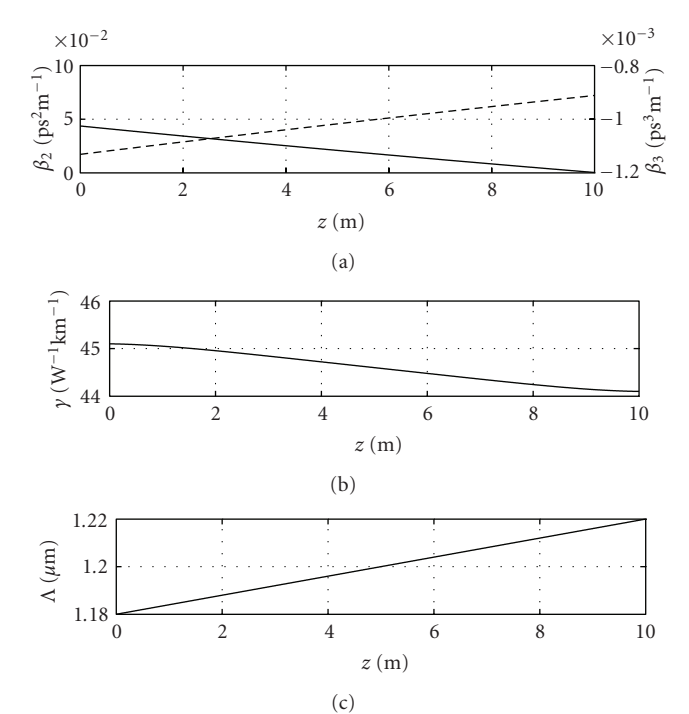


FIGURE 8: (a) β_2 and β_3 (- -) versus distance, (b) γ versus distance, and (c) pitch (Λ) versus distance, when $d/\Lambda = 0.3$.

FIGURE 9: (a) β_2 and β_3 (- -) versus distance, (b) γ versus distance, and (c) pitch (Λ) versus distance, when $d/\Lambda = 0.8$.

The initial pulse launched into the fibre was a Gaussian pulse with various peak powers and temporal widths. We choose a taper length $z_{\rm max}=10\,{\rm m}$ (this value determines slope of the linear taper profile in (5)), as this slope of the linear profile gives the best parabolic fit. We propagated the pulse along the taper from the narrow end, with $\Lambda=1.85\,\mu{\rm m}$ to $\Lambda=2.2\,\mu{\rm m}$, in the first case, when $d/\Lambda=0.3$. The range of input pulse peak power was 2 KW to 20 KW, and the range of input pulse FWHM was 200 femtoseconds to 5 picosecods. The range of input pulse peak powers and widths ensured

nonlinear propagation in all cases and prevented pulse distortion at higher pulse energies.

It has been shown in [7] that pulse reshaping is possible using nonlinear propagation in a length of a normally dispersive step index fibre. The best misfit parameter obtained in that study was 0.033, for a pulse energy of 31 pJ. Thus, for our method to be useful, we need to improve upon this figure. In fact, we find that for a range of parameters the minimum misfit parameter for different input energies is less than 0.002—for the example chosen, when $d/\Lambda = 0.8$, it is 0.0015. By carefully adjusting input pulse peak power and width, it is

	Λ [μm]	$\beta_2 [ps^2/m]$	$\beta_3 [ps^3/m]$	γ [W ⁻¹ km ⁻¹]
Start	1.18	0.0436	-0.001131	45.1
End	1.22	0.00031	-0.0009118	44.1

Table 2: Parameters of the tapered fibre $(d/\Lambda = 0.8)$.

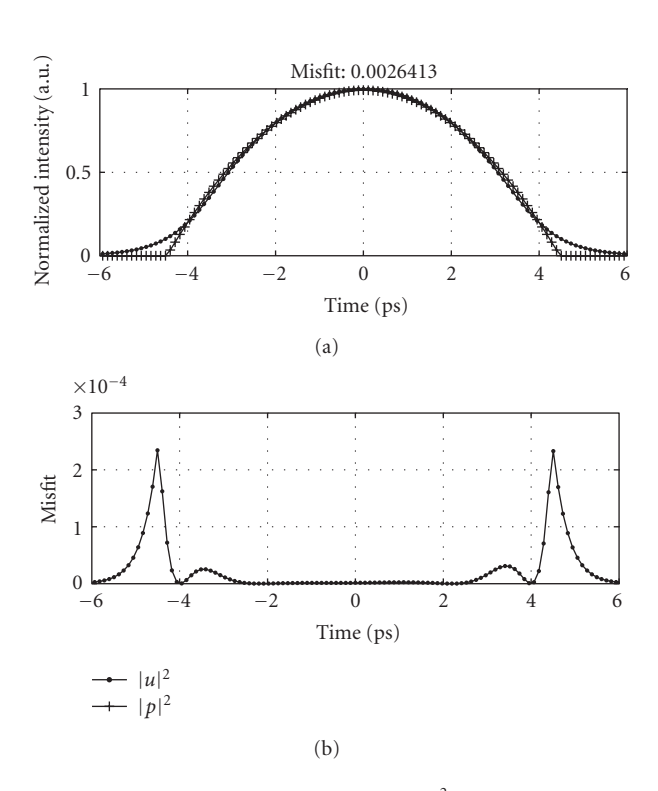


FIGURE 10: (a) Pulse envelope (normalize $|u|^2$) against parabolic fit (normalized $|p|^2$), and (b) local misfit parameter, $d/\Lambda = 0.3$.

possible to reach values corresponding to $M^2 < 0.001$, that is, significantly better than that obtained by a step index fibre.

A typical result is presented in Figure 10 which shows a plot of the intensity profile of the output pulse for a taper length of 2.2 m (peak power 2.8 KW and the pulse FWHM width 4.5 picoseconds) and the best parabolic fit, as well as plot of the local misfit. The pulse envelope is almost perfectly parabolic, apart from the pulse edges, as expected. The local misfit parameter is of the order of 10^{-4} which should be acceptable for most applications.

The minimum values of M^2 along the length of the taper (for $d/\Lambda=0.3$) are shown in Figure 11 assuming no loss for different initial conditions. Figure 12 shows distance along the taper where the misfit parameter has its minimum value. Similarly, Figure 13 shows the result obtained for the same taper with an artificially high-fibre loss taken into account as $\alpha=0.5$ dB/m. Also, Figure 14 shows distances that correspond to the minimum misfit parameter from Figure 13. Comparing these two sets of graphs, only minor differences can be seen showing that realistic fibre losses will not significantly affect the parabolic pulse generation. From Figures 11 and 12, or from Figures 13 and 14, we can extract the taper length that will provide the best misfit parameter, that is,

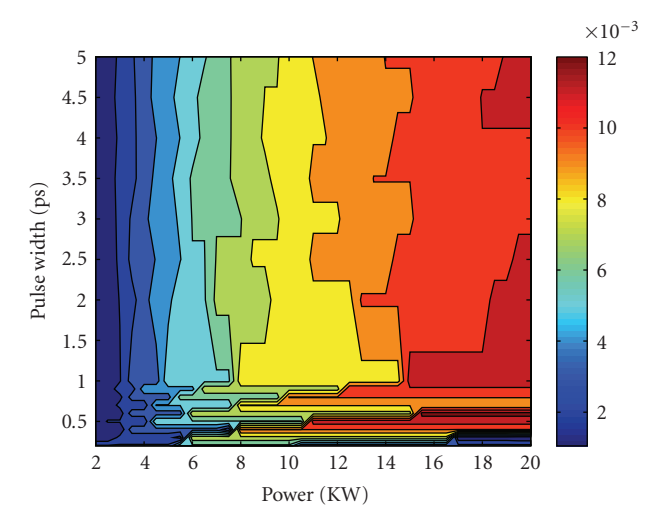


FIGURE 11: Misfit parameter (minimum) for input Gaussian pulse: $\alpha = 0$, $d/\Lambda = 0.3$.

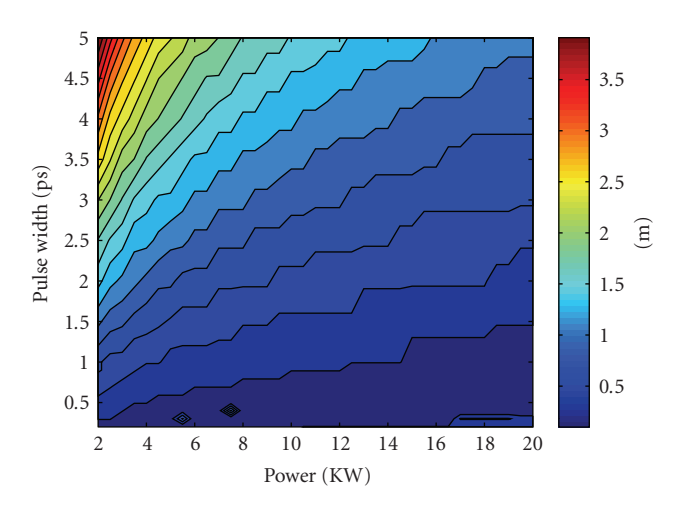


FIGURE 12: Taper length where the best (minimum) misfit parameter is obtained for input Gaussian pulse: $\alpha = 0$, $d/\Lambda = 0.3$.

where the best parabolic pulse is generated. From the contour plots given, it can be concluded that there is a range of values of input pulse widths and powers that will enable generation of parabolic pulses. Minimum value of misfit parameter, from Figure 11, is 0.002, obtained for input powers of around 3 KW, for different input pulse widths. From Figure 11, it can be seen that misfit parameter is a function of the peak power whilst it is mostly independent on the value of the pulse width. The taper length that corresponds to the chosen pulse peak power and width can be determined from Figure 12. Therefore, from Figures 11 and 12, it is possible to choose values for input pulse power, width, and the taper length

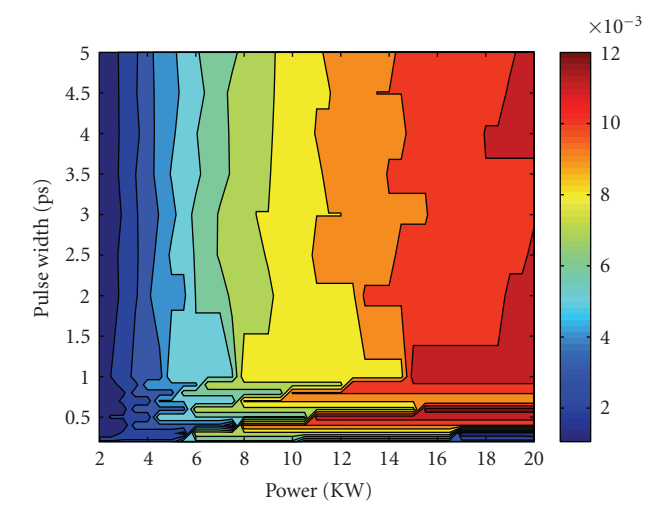


FIGURE 13: Misfit parameter (minimum) for input Gaussian pulse: $\alpha = 0.5$ dB/m, $d/\Lambda = 0.3$.

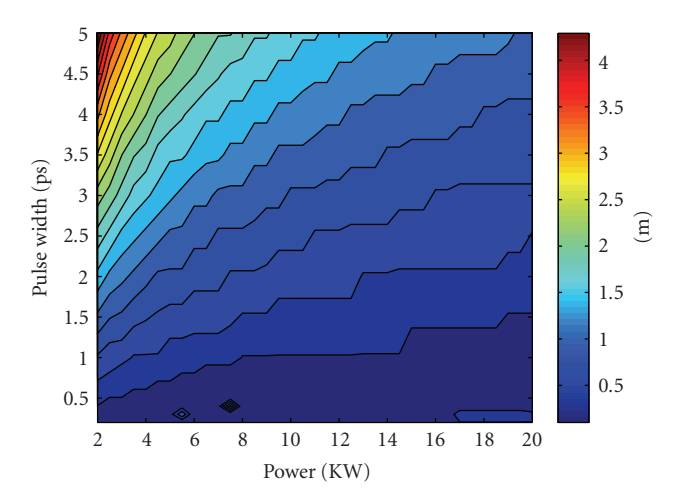


FIGURE 14: Taper length where the best (minimum) misfit parameter is obtained for input Gaussian pulse: $\alpha = 0.5$ dB/m, $d/\Lambda = 0.3$.

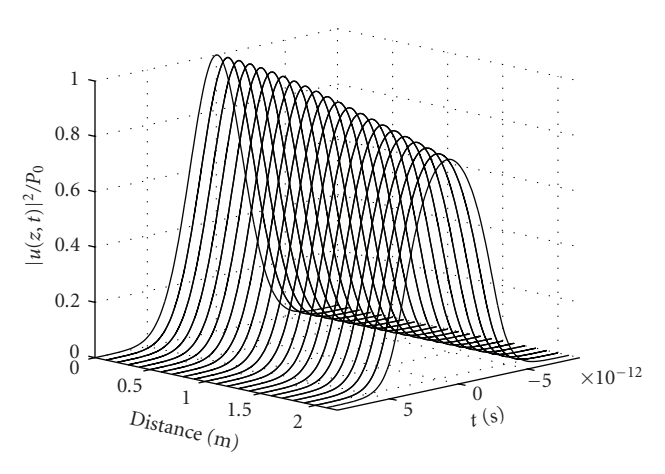


Figure 15: Parabolic pulse evolution, $d/\Lambda = 0.3$.

(this choice depends on the choice of the equipment used in the particular application). For the illustration purposes, we chose input pulse power, width, and the taper length: P_0 = 2.8 KW, T_0 = 4.5 picoseconds, and $Z_{\rm max}$ = 2.2 m, respectively. Figure 15 shows parabolic pulse evolution for the chosen parameters of the taper, when d/Λ = 0.3 and peak power P_0 = 2.8 KW, FWHM width T_0 = 4.5 picoseconds and the taper length $Z_{\rm max}$ = 2.2 m.

Figure 16 shows the pulse envelope, spectrum, phase, and chirp, for the chosen values. The spectra broadening factor is calculated as $B/B_0 = 28$ (where B is bandwidth at $z_{\rm max} = 2.2$ m, and B_0 is bandwidth, when z = 0 m). From the bottom plot in Figure 16, which represents instantaneous frequency, or chirp, it can be seen that the generated parabolic pulse has a linear chirp across it and therefore can be useful for practical applications. Figure 17 shows the result of the pulse compression performed numerically (using ideal pulse compression), where initial pulse full-width at half maximum (FWHM) is 4.5 picoseconds and after compression 310 femtoseconds, so that a compression ratio (calculated as the ratio of the FWHM of the input pulse to that of the compressed pulse) of 14.5 is obtained.

For the second taper, when $d/\Lambda = 0.8$, as the nonlinearity is much higher than when $d/\Lambda = 0.3$, the range of input pulse peak power was 10 W to 1 KW and the range of input pulse FWHM was 200 femtoseconds to 5 picoseconds. As for the first taper, we plotted contour plots of the minimum misfit parameter along the taper length (see Figure 18) and the corresponding distances (Figure 19) versus pulse peak powers and FWHM widths. From Figures 18 and 19 (as in the previous case), we could extract the information about the taper length which will provide the best misfit parameter. Minimum value of misfit parameter, from Figure 18, is 0.002, obtained for input powers of around 0.1 KW, for different input pulse widths. The taper length that corresponds to the chosen pulse peak power and width can be determined from Figure 19. Therefore, from Figures 18 and 19, it is possible to choose values for input pulse peak power, width, and the taper length: $P_0 = 0.1$ KW, $T_0 = 2$ picoseconds, and $z_{\text{max}} =$ 2.3 m, respectively. Similarly to the taper, when $d/\Lambda = 0.3$, from the contour plots given, it can be concluded that there is a range of values of input pulse widths and powers that will enable generation of parabolic pulses.

Figure 20 shows parabolic pulse evolution for the chosen parameters of the taper, when $d/\Lambda = 0.8$ and peak power $P_0 = 0.1$ KW, FWHM width $T_0 = 2$ picoseconds, and the taper length Z = 2.3 m.

Figure 21 shows the pulse envelope, spectrum, phase and chirp, for the taper, when $d/\Lambda = 0.8$, and the chosen values for the peak power, FWHM width, and the taper length. The spectra broadening factor is calculated as $B/B_0 = 9.25$, when $d/\Lambda = 0.8$. Result of the numerical pulse compression is shown in Figure 22. Initial pulse FWHM is 2 picoseconds and pulse is compressed to 332 femtoseconds, so that compression factor of 6 is obtained for this case. The sidelobes observed in Figures 17 and 22 are the theoretical wings of a recompressed parabolic pulse.

In Figure 23, for $d/\Lambda = 0.8$, we present the pulse envelope at the taper length 2.3 m, $P_0 = 0.1$ KW, and $T_0 = 2$

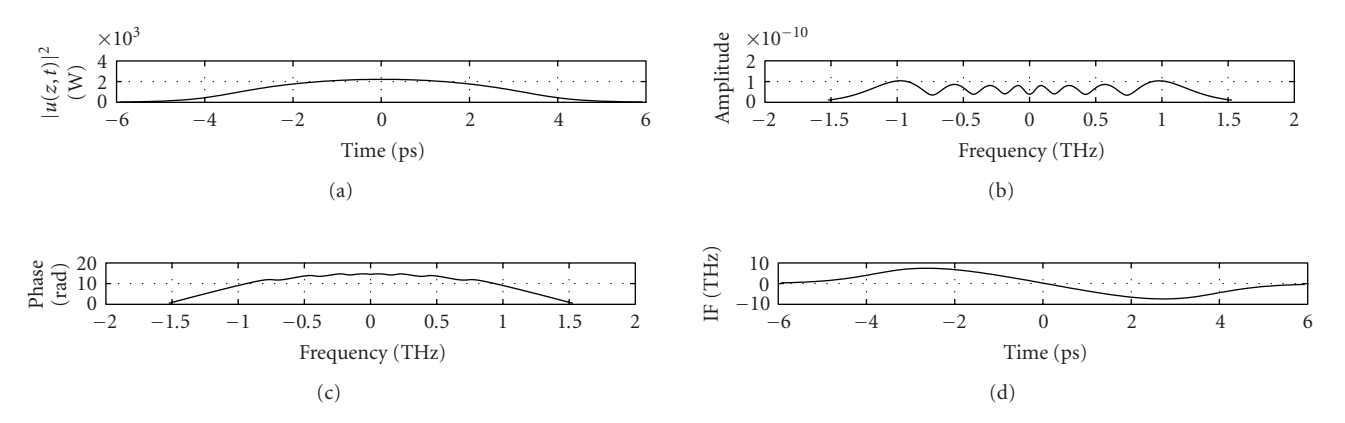


FIGURE 16: Pulse envelope, spectrum, phase, and chirp coefficients, $d/\Lambda = 0.3$.

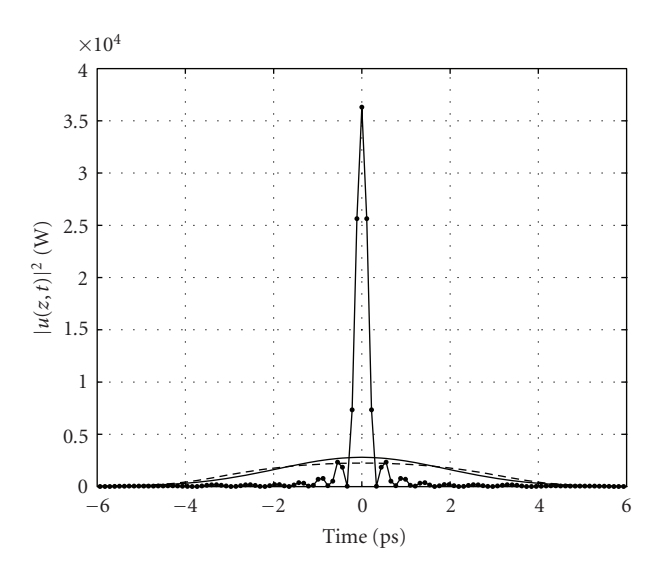


Figure 17: Initial pulse envelope, compressed pulse envelope (\bullet), and parabolic pulse (- -).

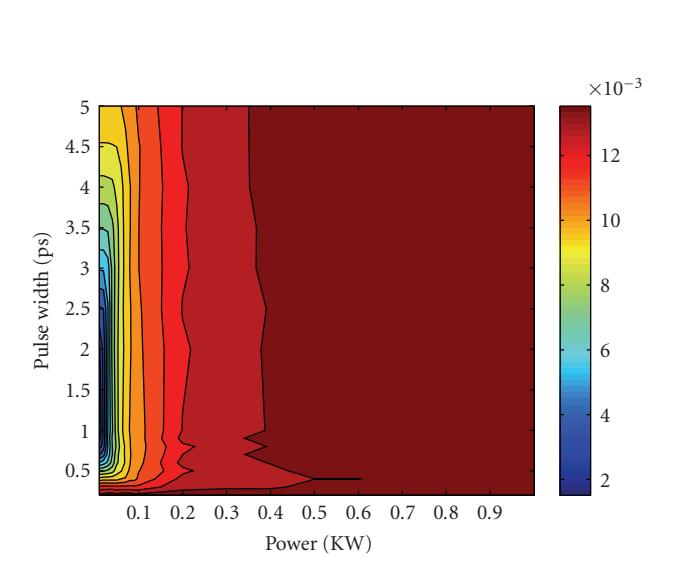


FIGURE 18: Misfit parameter (minimum) for input Gaussian pulse, $d/\Lambda = 0.8$.

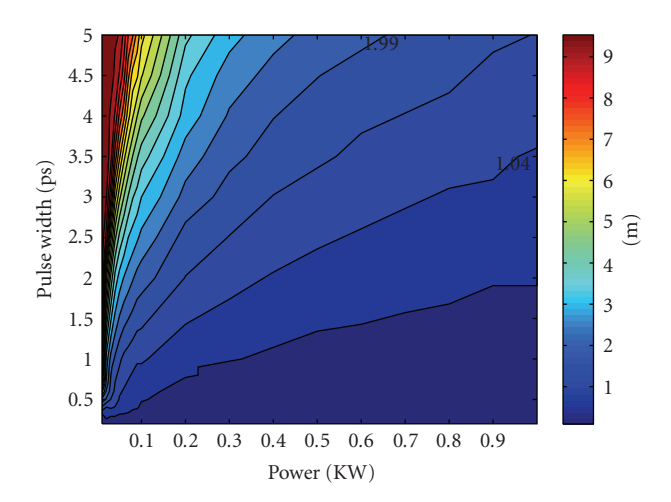


FIGURE 19: Taper length where the best (minimum) misfit parameter is obtained for input Gaussian pulse, $d/\Lambda = 0.8$.

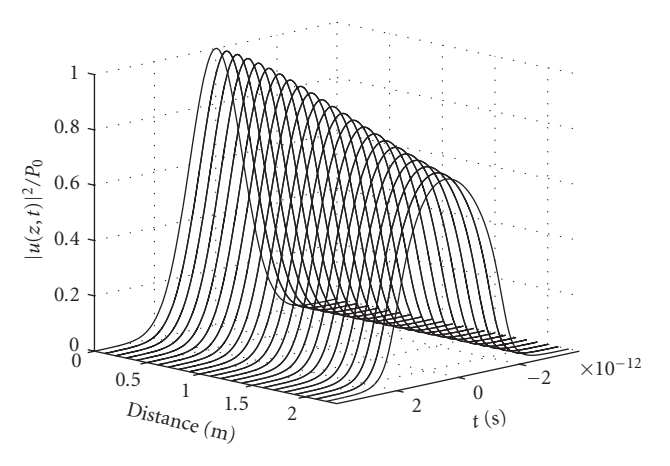


Figure 20: Parabolic pulse evolution, $d/\Lambda = 0.8$.

picoseconds and at the bottom plot, the misfit parameter or the error between the pulse intensity profile and the parabolic fit calculated using (8). It can be seen that the pulse exhibits the parabolic intensity profile, but with the

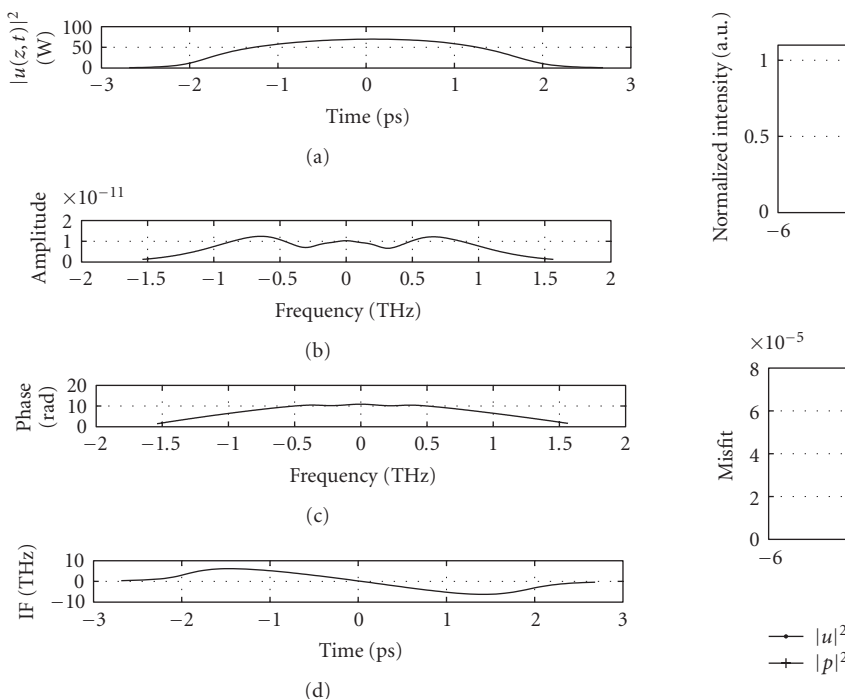


FIGURE 21: Pulse envelope, spectrum, phase and chirp coefficients, $d/\Lambda = 0.8$.

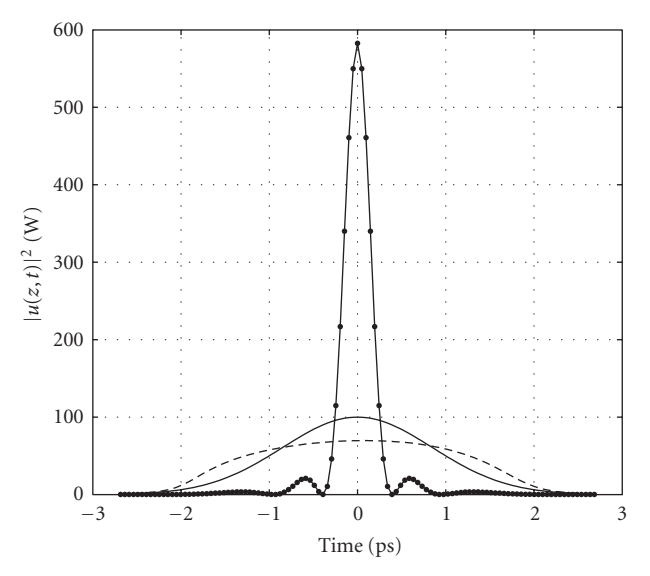


FIGURE 22: Initial pulse envelope, compressed pulse envelope (•), and parabolic pulse (- -).

small discrepancy in the wings of the pulse. By comparison of Figures 23 and 10, it can be observed that the minimum misfit parameter has a lower value when $d/\Lambda = 0.8$, so the intensity profile of the pulse for the taper when $d/\Lambda = 0.8$ deviates less from the parabolic shape in comparison to the case, when $d/\Lambda = 0.3$, although it deviates slightly more at the top of the pulse. We anticipate that this asymmetric deviation from the parabolic shape is due to the value of the third-order dispersion, which is nearly one order of magni-

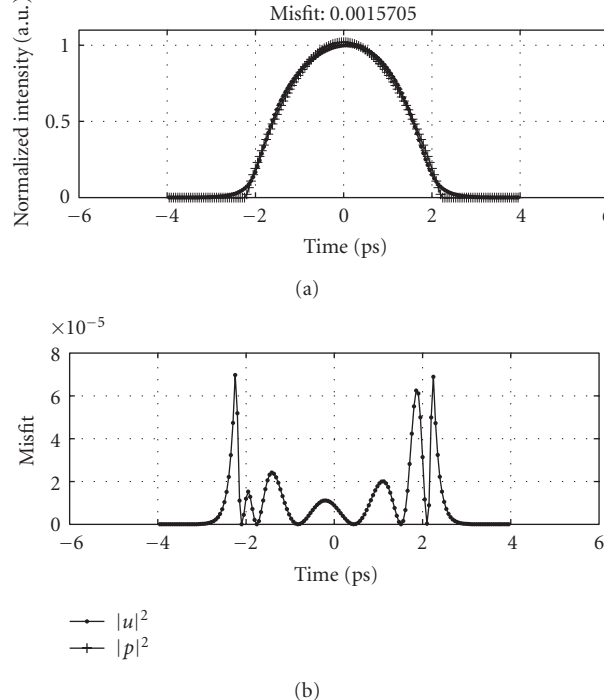


FIGURE 23: (a) Pulse envelope (normalized $|u|^2$) against parabolic fit (normalized $|p|^2$), and (b) local misfit parameter, $d/\Lambda = 0.8$.

tude higher, when $d/\Lambda = 0.8$, in comparison to the case $d/\Lambda = 0.3$. Also, the higher power of the pulse, when $d/\Lambda = 0.3$, is another reason for this greater misfit.

4. CONCLUSION

We have presented results of modelling and simulation of a microstructured optical fibre taper, where the parameters of the pitch and the air-filling factor are determined so that the normal dispersion regime is obtained. For two different values of the air-filling factor 0.3 and 0.8, two different tapers with a linear profile are proposed. In the case when d/Λ = 0.3, the confinement loss is non-negligible, so it has been taken into consideration. Results show that a Gaussian input pulse of different peak powers and widths can evolve into the parabolic shape with a linear chirp coefficient in both cases. The two different spectra broadening factors are calculated for two different cases, 28 when $d/\Lambda = 0.3$ and 9.25 when d/Λ = 0.8. Also, results show that using the first taper, when d/Λ = 0.3, linearly chirped parabolic pulse of FWHM width of 4.5 picoseconds can be compressed down to 310 femtoseconds, so that compression factor of 14.5 is achieved, and for the second taper, when $d/\Lambda = 0.8$, initial pulse FWHM width of 2 picoseconds is compressed to 332 femtoseconds, so that compression factor 6 is obtained. The optimal taper length, to achieve the best parabolic characteristic for a range of input powers and pulse widths, has also been determined. Results show that due to the different nonlinearity parameters for the two tapers under consideration, the best parabolic fit can be achieved for different pulse energies. When $d/\Lambda = 0.3$,

minimum misfit parameter is achieved for pulse energy in range from 10 nJ to 24 nJ, while when $d/\Lambda = 0.8$, due to the higher nonlinearity coefficient, the pulse energy range that gives minimum misfit parameter is from 177 pJ to 440 pJ. Therefore, we can conclude that these results might be of interest where pulse reshaping is conditioned by the initial pulse energy availability. Based on the presented procedure, optimization can be performed to find the best possible taper profile and length for the parabolic pulse generation.

REFERENCES

- [1] D. Anderson, M. Desaix, M. Karlsson, M. Lisak, and M. L. Quiroka-Teixeiro, "Wave-breaking-free pulses in nonlinear-optical fibers," *Journal of the Optical Society of America B*, vol. 10, no. 7, pp. 1185–1190, 1993.
- [2] F. Parmigiani, P. Petropoulos, M. Ibsen, and D. J. Richardson, "Pulse retiming based on XPM using parabolic pulses formed in a fiber bragg grating," *IEEE Photonics Technology Letters*, vol. 18, no. 7, pp. 829–831, 2006.
- [3] M. Nakazawa, T. Hirooka, F. Futami, and S. Watanabe, "Ideal distortion-free transmission using optical Fourier transformation and Fourier transform-limited optical pulses," *IEEE Photonics Technology Letters*, vol. 16, no. 4, pp. 1059–1061, 2004.
- [4] F. Parmigiani, C. Finot, K. Mukasa, et al., "Ultra-flat SPM-broadened spectra in a highly nonlinear fiber using parabolic pulses formed in a fiber Bragg grating," *Optics Express*, vol. 14, no. 17, pp. 7617–7622, 2006.
- [5] A. Ruehl, O. Prochnow, M. Schultz, D. Wandt, and D. Kracht, "Impact of third-order dispersion on the generation of wavebreaking free pulses in ultrafast fiber lasers," *Optics Letters*, vol. 32, no. 17, pp. 2590–2592, 2007.
- [6] T. Hirooka and M. Nakazawa, "Parabolic pulse generation by use of a dispersion-decreasing fiber with normal groupvelocity dispersion," *Optics Letters*, vol. 29, no. 5, pp. 498–500, 2004.
- [7] C. Finot, L. Provost, P. Petropoulos, and D. J. Richardson, "Parabolic pulse generation through passive nonlinear pulse reshaping in a normally dispersive two segment fiber device," Optics Express, vol. 15, no. 3, pp. 852–864, 2007.
- [8] C. Finot, B. Barviau, G. Millot, A. Guryanov, A. Sysoliatin, and S. Wabnitz, "Parabolic pulse generation with active or passive dispersion decreasing optical fibres," *Optics Express*, vol. 15, no. 24, pp. 15824–15835, 2007.
- [9] A. Plocky, A. A. Sysoliatin, A. I. Latkin, et al., "Experiments on the generation of parabolic pulses in waveguides with lengthvarying normal chromatic dispersion," *JETP Letters*, vol. 85, no. 7, pp. 319–322, 2007.
- [10] V. I. Kruglov, A. C. Peacock, J. D. Harvey, and J. M. Dudley, "Self-similar propagation of parabolic pulses in normaldispersion fiber amplifiers," *Journal of the Optical Society of America B*, vol. 19, no. 3, pp. 461–469, 2002.
- [11] F. Ö. Ilday, J. R. Buckley, W. G. Clark, and F. W. Wise, "Self-similar evolution of parabolic pulses in a laser," *Physical Review Letters*, vol. 92, no. 21, Article ID 213902, 4 pages, 2004.
- [12] B. Kibler, C. Billet, P.-A. Lacourt, R. Ferriere, L. Larger, and J. M. Dudley, "Parabolic pulse generation in comb-like profiled dispersion decreasing fibre," *Electronics Letters*, vol. 42, no. 17, pp. 965–966, 2006.
- [13] P. S. J. Russell, "Photonic-crystal fibers," *Journal of Lightwave Technology*, vol. 24, no. 12, pp. 4729–4749, 2006.

- [14] J. Hu, B. S. Marks, and C. Menyuk, "Pulse compression using a tapered microstructured optical fiber," *Optics Express*, vol. 14, no. 9, pp. 4026–4036, 2006.
- [15] M. L. V. Tse, P. Horak, J. H. V. Price, F. Poletti, F. He, and D. J. Richardson, "Pulse compression at 1.06 μm in dispersion-decreasing holey fibers," *Optics Letters*, vol. 31, no. 23, pp. 3504–3506, 2006.
- [16] T. A. Birks, W. J. Wadsworth, and P. S. J. Russell, "Supercontinuum generation in tapered fibers," *Optics Letters*, vol. 25, no. 19, pp. 1415–1417, 2000.
- [17] X. Liu, C. Xu, W. H. Knox, et al., "Soliton self-frequency shift in a short tapered air-silica microstructure fiber," *Optics Letters*, vol. 26, no. 6, pp. 358–360, 2001.
- [18] F. Poletti, K. Furusawa, Z. Yussoff, et al., "Nonlinear tapered holey fibers with high SBS threshold and controlled dispersion," *Journal of the Optical Society of America B*, vol. 24, no. 9, pp. 2185–2194, 2007.
- [19] D. J. Richardson, R. P. Chamberlin, L. Dong, and D. N. Payne, "High quality soliton loss compensation in 38 km dispersiondecreasing fibre," *Electronics Letters*, vol. 31, no. 19, pp. 1681– 1682, 1995.
- [20] D. J. Richardson, R. P. Chamberlin, L. Dong, and D. N. Payne, "Experimental demonstration of 100 GHz dark soliton generation and propagation using a dispersion decreasing fibre," *Electronics Letters*, vol. 30, no. 16, pp. 1326–1327, 1994.
- [21] A. I. Latkin, S. K. Turitsyn, and A. A. Sysoliatin, "Theory of parabolic pulse generation in tapered fiber," *Optics Letters*, vol. 32, no. 4, pp. 331–333, 2007.
- [22] F. Zolla, G. Renversez, A. Nicolet, B. Kuhlmey, S. Guenneau, and D. Felbacq, *Photonic Crystal Fibres*, Imperial College Press, London, UK, 2005.
- [23] G. P. Agrawal, *Nonlinear Fiber Optics*, Academic Press, San Francisco, Calif, USA, 2nd edition, 1995.
- [24] P. R. McIsaac, "Symmetry-induced modal characteristics of uniform waveguides I: summary of results," *IEEE Transactions* on Microwave Theory and Techniques, vol. 23, no. 5, pp. 421– 429, 1975.
- [25] T. E. Murphy, simulation software SSPROP, University of Maryland, www.photonics.umd.edu/software/ssprop.